# Femtosecond Laser Ablation Molecular Isotopic Spectrometry for Zirconium Isotope Analysis

**ARTICLE** *in* ANALYTICAL CHEMISTRY · MARCH 2015

Impact Factor: 5.64 · DOI: 10.1021/acs.analchem.5b00056 · Source: PubMed



**6 AUTHORS**, INCLUDING:

Huaming Hou
Lawrence Berkeley National Laboratory
**20** PUBLICATIONS **65** CITATIONS
SEE PROFILE

Xianglei Mao
Lawrence Berkeley National Laboratory
**167** PUBLICATIONS **4,682** CITATIONS
SEE PROFILE

Vassilia Zorba
Lawrence Berkeley National Laboratory
**63** PUBLICATIONS **1,171** CITATIONS
SEE PROFILE

Ronger Zheng
Ocean University of China
**76** PUBLICATIONS **239** CITATIONS
SEE PROFILE

analytical chemistry

Article

pubs.acs.org/ac

# Femtosecond Laser Ablation Molecular Isotopic Spectrometry for Zirconium Isotope Analysis

Huaming Hou,[†,‡] George C.-Y. Chan,[†] Xianglei Mao,[†] Vassilia Zorba,[†] Ronger Zheng,[‡] and Richard E. Russo*[,†]

[†]Lawrence Berkeley National Laboratory, Berkeley, California 94720, United States

[‡]Ocean University of China, Qingdao, 266100, People's Republic of China

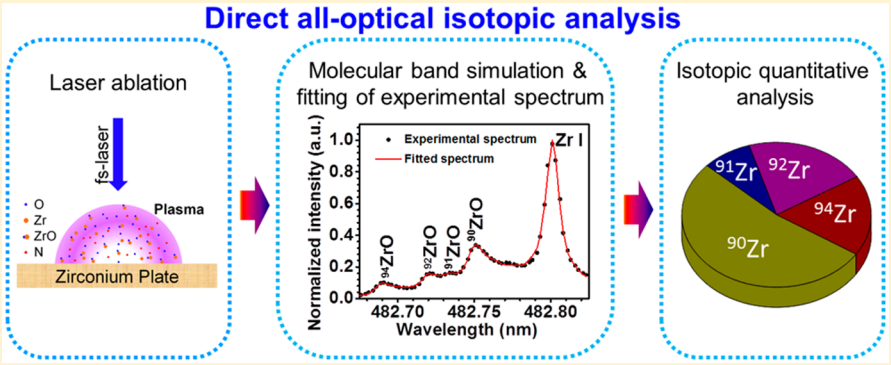


**ABSTRACT:** Laser ablation molecular isotopic spectrometry (LAMIS) for rapid isotopic analysis of zirconium at atmospheric pressure was studied with a femtosecond-laser system operated under high repetition rate (1 kHz) and low pulse energy (160 $\mu$J). The temporal evolution of zirconium neutral-atomic and ionic lines, as well as zirconium oxide molecular bands, were studied. Six molecular bands, belonging to the $d^3\Delta-a^3\Delta$ (i.e., the $\alpha$ system) and $E^1\Sigma^+-X^1\Sigma^+$ transitions, were observed with appreciable isotopic shifts. The assignments of the isotopic bandheads were first based on theoretical predictions of the band origins and the associated isotopic shifts of various dipole-allowed ZrO electronic transitions, followed by an experimental confirmation with a $^{94}$Zr-enriched $ZrO_2$ sample. In this work, the $\alpha(0,1)$ band from the $d^3\Delta_3-a^3\Delta_3$ subsystem was utilized for Zr isotope analysis based on a compromise between the magnitude of isotopic shifts in emission wavelengths, emission strengths, signal-to-background ratios, and spectral interferences. The analysis was performed in a standardless calibration approach; the isotopic information was extracted from the experimentally measured molecular spectra through theoretical spectral fitting. The results demonstrate the feasibility to obtain isotopic information for a spectrally complicated element like zirconium, without the need to use isotopically labeled calibration standards. The availability of comprehensive molecular constants will further improve the analytical accuracy of this standardless calibration approach.

Laser-induced breakdown spectroscopy (LIBS), in which a plasma is generated through focusing a pulsed laser onto the surface of a solid target or inside a liquid or gaseous sample,[1,2] has been advanced as an analytical technique over the past several decades.[3,4] The laser-ablated sample undergoes vaporization, atomization, ionization, and excitation in the plasma plume, and the excited species emit at their characteristic wavelengths. As the emission lines in the plasma plume contains the chemical fingerprint of the sample, chemical characterization is performed by analyzing the emission spectrum. One feature of LIBS is its capability to perform the analysis in a standoff fashion, with the laser and spectrometer well-removed from the sample. This unique capability is particularly attractive for nuclear forensics as it allows detection, identification, and quantification of suspicious (and potentially radioactive) samples at remote distances and provides spectral signatures indicative of nuclear proliferation in real time.

Although different isotopes of the same element also emit at slightly different wavelengths, most LIBS analyses are performed to determine only the elemental content of samples because isotopic shifts in atomic transitions for most elements (except very light or heavy elements[5]) are too small to be practically resolved. The recent development of laser ablation molecular isotopic spectrometry (LAMIS),[6,7] which allows the determination of isotopic ratios in a sample,[8,9] expands the capability of direct chemical analysis by laser ablation. All advantages associated with LIBS (e.g., rapid, multielemental analysis, no sample preparation, capability of in situ or stand-off analysis, and spatially resolved analysis[1,4]) also apply to LAMIS. Isotopic analyses of hydrogen, boron, carbon, and strontium with the LAMIS technique were discussed in our previous

**Received:** January 6, 2015
**Accepted:** March 30, 2015
**Published:** March 30, 2015





DOI: 10.1021/acs.analchem.5b00056
*Anal. Chem.* 2015, 87, 4788−4796

papers.[6,7,10,11] With the exception of Sr, which we analyzed the isotopic spectra from its four isotopes, all other LAMIS works were performed for the analysis of two isotopes. The molecular isotopic shifts for hydrogen, boron, and carbon are comparatively large—a characteristics of light elements. Although the atomic weights of Sr are comparable to Zr, the present work differs from our previous Sr work in two aspects. First, we previously showed the qualitative comparison of spectral features of several Sr isotopes in SrO, SrBr, SrF, and SrI, but no quantitative isotope analysis of Sr was involved in that study. Second, the atomic/ionic spectra from Sr are relatively simple and no interference of Sr atomic lines on strontium diatomic molecules was observed, which is in great contrast to the line-rich Zr.

In this study, we evaluated the performance of LAMIS for isotopic analysis of a spectrally rich element—zirconium. Like any emission technique,[12,13] the accuracy and precision of LAMIS could be compromised by the presence of spectral interference and background emission. In LAMIS, especially for line-rich elements, such spectral interference could arise from atomic emission of the element of interest (i.e., the LIBS signal) itself. As both the atomic line and molecular band emission from zirconium are spectrally dense, it is a good candidate to evaluate the performance of LAMIS under such spectral-rich conditions. Natural zirconium comprises five stable isotopes (with mass numbers 90, 91, 92, 94, and 96), which could be considered a challenging case for LAMIS. Isotopic analysis of zirconium is important in nuclear science and forensics.[14,15] For example, zirconium, in the form of zircaloys, is used as a cladding material for nuclear reactor fuels because of its low neutron-capture cross-section.[16,17] In nuclear forensics, because the maxima of the yields of fission products from thermal neutron-induced fission of $^{235}$U and $^{239}$Pu are found in the ranges of mass numbers 90−100 and 95−105, respectively,[18,19] Zr isotopic analysis allows the determination of the contribution of fissions from these two radionuclides.[20]

Isotopic analyses of Zr are typically carried out with mass spectrometry [e.g., thermal ionization mass spectrometry (TIMS) or inductively coupled plasma mass spectrometry (ICPMS)].[21,22] Conventional atomic emission by LIBS is not feasible to provide isotopic information on zirconium (as well as many other elements in the middle of the periodic table) because the isotopic shifts in atomic transitions are at least 1 order of magnitude lower than the typical line widths encountered in LIBS under atmospheric pressure due to various broadening mechanisms (e.g., Stark, Doppler, and pressure) in the plasma. For example, the isotopic shifts in atomic transitions between consecutive even isotopes of zirconium are typically in the range of 200 MHz and seldom more than 300 MHz (which translates to <0.1 pm for wavelength at 500 nm).[23] As will be demonstrated in this study, isotopic signatures from Zr are readily identified and quantified from its molecular oxide (ZrO) emission.

A means to improve the analytical performance of LAMIS is to optimize the laser ablation and spectral emission measurement parameters so that molecular emission is favored while atomic emission is suppressed. For example, gating the detector and measuring the LAMIS signal at a later time after the laser ablation pulse enhances the relative strengths of molecular over atomic emission.[7,10] For LAMIS with a typical nanosecond laser, molecular emission can persist for tens of microseconds after the laser pulse, when most of the plasma continuum and atomic emission have decayed considerably.[7,10] The use of femtosecond laser pulses was reported to enhance the emission from molecular over the atomic species, at least for nonmetallic molecular species.[24−26] Therefore, a fs-laser system was used in the present study.

We measured the temporally resolved atomic and molecular oxide emission from a zirconium metallic sample after fs-laser ablation, with particular emphasis on the emission intensity ratio of molecular band to atomic line. The best ZrO molecular band for LAMIS analysis was determined from the viewpoint of the magnitude of isotopic shifts in emission wavelengths, emission strengths, signal-to-background ratios, as well as spectral overlaps with atomic lines of Zr and other ZrO bands. As will be shown later, the $\alpha(0,1)$ band of $d^3\Delta_3$–$a^3\Delta_3$ system was the optimum one overall. Isotopic analysis was performed in a standardless calibration approach by fitting the experimental acquired spectra with a set of theoretical synthetic spectra.

## EXPERIMENTAL SECTION

**Experimental Setup.** The femtosecond laser was an amplified diode-pumped ytterbium-doped system (s-pulse, Amplitude Systems). It delivered approximately 500 fs pulses at a repetition of 1 kHz. The laser frequency was tripled to an output wavelength at 343 nm. Laser energy was measured with an energy meter (OPHIR PE10-C) at 160 $\mu$J/pulse, corresponding to an average power of 0.16 W. The laser beam was focused onto the sample (a zirconium metal plate, 99.2%, Alfa Aesar) by a microscope objective lens with a working distance of 49 mm (LMU-3X-UVB, Thorlabs). To confirm the isotopic assignment of the ZrO bandheads, a $^{94}$Zr-enriched zirconium dioxide ($ZrO_2$) sample (with 97+% $^{94}$Zr, Trace Science International, ON, Canada) was used. This $^{94}ZrO_2$ sample was prepared by pressing the $ZrO_2$ powder under 7 tons of force for 4 min into a 1 cm diameter pellet. All samples were mounted on a three-dimensional computer-controlled translation stage with adjustable motion speed. The sample surface was adjusted to be 2 mm above the focal point for maximum plasma emission. The sample was continuously translated in its *XY*-plane during spectra acquisition.

Plasma emission was collected and focused onto an optical fiber bundle with a fused-silica plano-convex lens ($f$ = 35 mm). The other end of the fiber bundle was coupled onto the entrance slit of a Czerny−Turner spectrometer (focal length = 1.25 m, Horiba JY 1250M) with an intensified charge-coupled device (ICCD) (PI MAX 1024, Princeton Instruments) as the detector. A grating with groove density of 3600 per mm was used, resulting in a spectral resolution of 15 pm. The dark current of the detector was recorded either immediately before or after each experiment, and all presented data are dark-current subtracted. Flatfield correction for the ICCD was also performed.[27] Wavelengths were calibrated with an Fe−Ne hollow cathode lamp.[28] Time-resolved measurements of the plasma emission evolution were studied by varying the delay time of the ICCD.

**Simulation of ZrO Molecular Emission and Isotopic Analysis.** The wavelengths of molecular emission depend on the vibrational and rotational energy levels within the two electronic transition states. It is well-known that replacing one atom with its isotope in a diatomic molecule can appreciably change the vibrational and rotational energy levels of the molecule.[29,30] As a result, molecules constitute different isotopes emitting at slightly different wavelengths and LAMIS


DOI: 10.1021/acs.analchem.5b00056
*Anal. Chem.* 2015, 87, 4788−4796

exploits this shift for isotopic analysis. This isotopic shift (in terms of energy, $\Delta\upsilon$) can be expressed as[6]

$$\Delta\upsilon = (1-\rho)\left[\omega_e'\left(\nu'+\frac{1}{2}\right)-\omega_e''\left(\nu''+\frac{1}{2}\right)\right] - (1-\rho^2)\left[\omega_e'x_e'\left(\nu'+\frac{1}{2}\right)^2-\omega_e''x_e''\left(\nu''+\frac{1}{2}\right)^2\right] + (1-\rho^2)[B_v'J'(J'+1)-B_v''J''(J''+1)] \quad (1)$$

where $\omega_e$ and $\omega_e x_e$ are the vibrational and anharmonicity constants, respectively; $B_v$ is the rotational constant; $\nu$ and $J$ are the vibrational and rotational quantum numbers, respectively. The single and double primed symbols refer to the upper and lower energy levels, respectively; $\rho$ is defined as $(\mu_{ref}/\mu_i)^{1/2}$, in which $\mu$ is the reduced mass of the molecule, and subscripts ref and $i$ denote the reference and all other isotopes, respectively. The reference isotope is typically the one with the highest natural abundance (i.e., $^{90}$Zr in this case).

In this study, the ZrO $\alpha(0,1)$ band of the $d^3\Delta_3$–$a^3\Delta_3$ subsystem was employed for isotopic determination of Zr, based on an optimization among various measurable ZrO molecular bands. The theoretical spectrum for $^{90}$ZrO can be calculated from the reported molecular spectroscopic constants.[31,32] The spectra for other Zr isotopes ($^{94}$Zr, $^{92}$Zr, and $^{91}$Zr) are then calculated from the corresponding $\rho$ values.[33] As will be discussed, peaks from $^{96}$ZrO are heavily blended with rotational structures from other ZrO bands emitting at similar wavelengths, and therefore, $^{96}$ZrO is omitted in the fitting. Also, we found that the isotopic shifts of the ZrO $d^3\Delta_3$– $a^3\Delta_3$ (0,1) band show appreciable deviation from the theoretically predicted values due to a possible energy-level perturbation. Therefore, we tuned the $\rho$ values for each Zr isotope based on our experimental spectra for the fitting. The intensity distribution of each rotational component was calculated based on rotational line strengths (i.e., the Hönl–London factors[34]) with a Boltzmann distribution under a certain temperature.

Isotopic information on the sample was extracted by fitting the experimental with synthetic emission spectra. The algorithm was based on our previously reported approach[35,36] with two modifications to further improve the fitting. First, the synthetic spectra contain not only the ZrO molecular emission [denoted as $I^{syn}_{ZrO}(\lambda)$], but also a nearby Zr atomic line [Zr I 482.804 nm, denoted as $I^{syn}_{Zr\text{-}atomic}(\lambda)$]. The spectral profile of the Zr I line is assumed to be Lorentzian, with both the peak width and amplitude as fitting parameters. Second, because the peak intensity of this Zr atomic line was stronger than that of the ZrO bandhead, a weighting procedure was performed to ensure that the fitting was not focused only on this stronger Zr atomic line. The intensities of all data points in the section of the spectrum to be fitted were first sorted, and a reference value ($I_{weight\text{-}ref}$) corresponding to a user-selectable percentile level (currently at 40%) was found. The weighing ($w$) for each data point in the fitting was then assigned based on its intensity ($I_i$)

$$w = \begin{cases} 1, & \text{if } I_i \le I_{weight\text{-}ref} \\ \dfrac{I_{weight\text{-}ref}}{I_i}, & \text{otherwise} \end{cases} \quad (2)$$

The synthetic spectra for ZrO takes the following form

$$I^{syn}_{ZrO}(\lambda) = c_{90Zr}I^{syn}_{90ZrO}(\lambda) + c_{91Zr}I^{syn}_{91ZrO}(\lambda) + c_{92Zr}I^{syn}_{92ZrO}(\lambda) + c_{94Zr}I^{syn}_{94ZrO}(\lambda) \quad (3)$$

The ratio of the coefficients $c_{90Zr}/c_{91Zr}/c_{92Zr}/c_{94Zr}$ corresponds to the isotopic abundance ratio of Zr in the sample. The fitting algorithm locates the best combination of all fitting parameters by minimization of the sum of the squares of the fitting residuals [$\varepsilon(\lambda)$] at all wavelengths ($\lambda$) of the experimental spectrum, $I^{expt}(\lambda)$, through

$$I^{expt}(\lambda) = I^{syn}_{ZrO}(\lambda) + I^{syn}_{Zr\text{-}atomic}(\lambda) + I_{continuum} + \varepsilon(\lambda) \quad (4)$$

## RESULTS AND DISCUSSION

**Sample Translational Speed.** As laser ablation proceeds, mass is removed from the sample and an ablation crater develops. With repetitive ablation at one location, both the physical characteristics of the plasma and the mass removal rate (and hence the LIBS and LAMIS signals) change.[37] In order to obtain a stable emission signal, the laser sampling location can be translated at a properly selected speed so that the crater depth is controlled. Figure 1 shows the variations of a Zr I signal during a data-acquisition sequence at various sample translation speeds. Each data point corresponded to an integration time of 1 s. Steady Zr I intensity was obtained only when the sample translation speed was increased to 0.1 mm/s. This sample translational speed was used for all other experiments described in this paper.

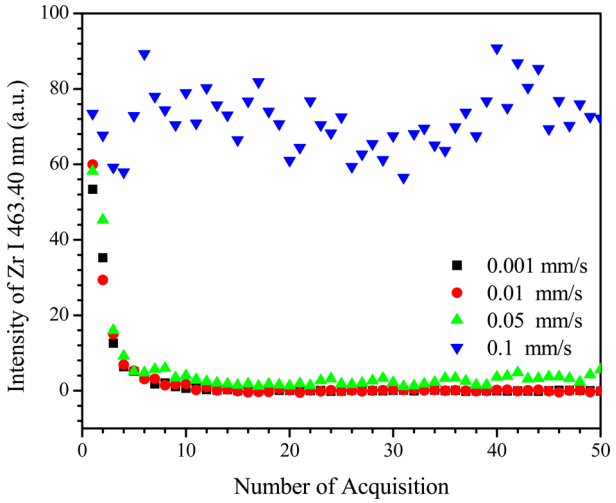


**Figure 1.** Influence of sample translational speed on Zr emission stability of femtosecond laser-ablated plasma. The exposure time for each data point was 1 s, which corresponded to 1000 laser shots. The ICCD gate delay and gate width were both set to 1 $\mu$s.

**Evolution of Laser-Induced Plasma Emission.** *Temporally Resolved Emission Spectra.* Figure 2 shows four time-resolved plasma emission spectra from a zirconium metal target over the 461.8–464.7 nm spectral range. The gate width of the ICCD was set the same as the ICCD delay time, and all spectra were normalized to the ICCD gate width (in unit of 100 ns). For example, to obtain the normalized intensity for spectra acquired with a gate width of 200 ns, the measured intensity was then divided by a factor of 2. The fs-laser was fired at 1000 Hz, and the spectra are an accumulation of 1000 laser pulses (i.e., 1 s exposure time). As early as a delay time of 100 ns, the spectrum is already dominated by discrete zirconium


DOI: 10.1021/acs.analchem.5b00056
Anal. Chem. 2015, 87, 4788–4796

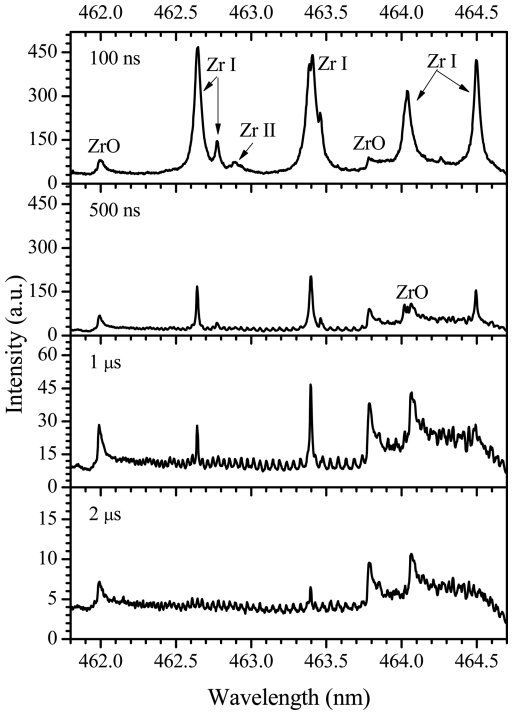


**Figure 2.** Temporally resolved femtosecond LIBS/LAMIS spectra of a Zr metallic sample from 461.8 to 464.7 nm. The indicated times in the figure represent the delay time of the ICCD. Gate width of the ICCD was set equal to gate delay. Emission intensities were normalized to gate width, in units of 0.1 $\mu$s.

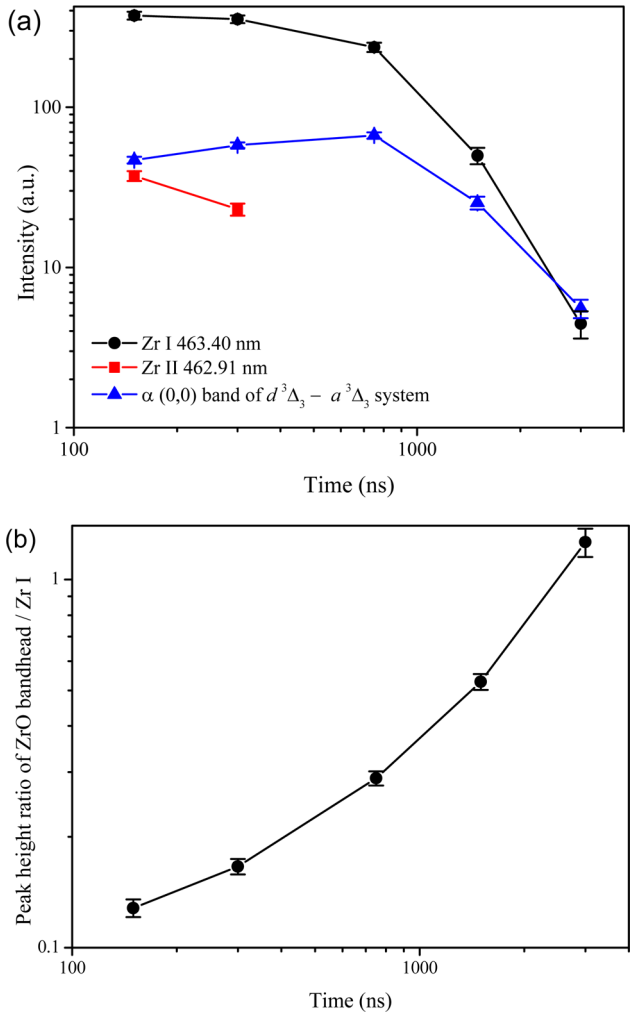


**Figure 3.** Temporally resolved emission from (a) Zr I 463.40 nm, Zr II 462.91 nm, and ZrO bandhead at 461.98 nm and (b) emission intensity ratio of ZrO bandhead at 461.98 nm to peak height of Zr I 463.40 nm line during laser ablation of a Zr metallic target. The ZrO bandhead at 461.98 nm belongs to the $\alpha(0,0)$ band of the $d^3\Delta_3$–$a^3\Delta_3$ subsystem.

neutral-atomic lines. The Zr I lines are broadened by the Stark effect. The ionic Zr II line at 462.91 nm is weak but distinguishable. Also, two ZrO bandheads are readily identified. These two bands belong to the $\alpha(0,0)$ system (the $d^3\Delta_3$–$a^3\Delta_3$ and $d^3\Delta_2$– $a^3\Delta_2$ subsystem, respectively) of ZrO.[38,39] The bandhead of the $d^3\Delta_1$–$a^3\Delta_1$ subsystem overlaps with a zirconium atomic line at 464.01 nm and becomes clearly observed only at a longer delay time of 500 ns. With a delay time of only 500 ns, the line widths of the Zr I lines become narrow and the Zr II line disappears. All three subsystems of the $\alpha(0,0)$ ZrO band can be observed. The rotational spectral features from the ZrO molecular band, which makes the baseline appear as ripples, are very clear. With further increase of the delay time to 1 $\mu$s, those atomic emission lines with high upper energy levels (e.g., Zr I 462.64 nm) decay faster than their lower energy counterparts (e.g., Zr I 463.46 nm). At longer delay time of 2 $\mu$s, Zr I lines almost completely disappear, and the molecular species dominate the emission.

*Characterization of Atomic and Molecular Emission.* The temporal evolution of the peak intensities of the Zr I 463.40 nm line, the Zr II 462.91 nm line, and the ZrO 461.98 nm molecular bandhead are summarized in Figure 3a. In this figure, time is defined as the center of the ICCD gate width, which was set the same as the gate delay with respect to the laser pulse. For example, for a gate delay and gate width setting of 2 $\mu$s, the center of the ICCD gate width corresponds to 3 $\mu$s after the laser pulse. Fifty spectra were acquired for each delay time studied, and the error bars represent their standard deviations. All intensities were normalized to the ICCD gate width. For the Zr I 463.40 nm line, strong (and also maximum) atomic emission was observed at a delay time of 150 ns and lasting up to 3 $\mu$s (cf. Figure 3a). Other measured Zr I lines (not shown) followed a similar trend. The evolution of the Zr II 462.91 nm ionic line is dramatically different compared to Zr I 463.4 nm atomic line. This line lasted only about 300 ns. Unlike the atomic and ionic lines which exhibited their maxima at early delay times, the maximum of ZrO emission occurred at a much later time (750 ns) (cf. Figure 3a). As expected, molecular formation is favored during cooling of the plasma. Similar observations were reported by Bai et al.[40] and Sarkar et al.[11] in their works with AlO and OH molecular emission, respectively.

As discussed in the introduction, one potential interference for LAMIS is from the atomic LIBS signal. Plasma conditions for LAMIS measurement should be chosen to favor molecular over atomic emission. Figure 3b shows the peak intensity ratios of the ZrO bandhead at 461.98 nm to the Zr I 463.40 nm line, which is the strongest and most persistent Zr line in the investigated wavelength range. The ratios expressed a monotonic raising trend with delay time, and the highest ZrO/Zr I ratio was 1.3. Although a longer detection gate delay minimizes spectral interferences from atomic lines over molecular bands, the emission strengths from the molecular bands also decline. As a compromise between maximum signal-


DOI: 10.1021/acs.analchem.5b00056
*Anal. Chem.* 2015, 87, 4788–4796

**Table 1. Predicted Band Origin of $^{90}$ZrO and Isotope Shifts for $^{94}$ZrO (with Respect to $^{90}$ZrO)**

| | band origin (nm) | | | isotopic shift (pm)[b] | | | |
|---|---|---|---|---|---|---|---|
| transitions[a] | (0,0) | (0,1) | (1,0) | (0,0) | (0,1) | (1,0) | ref[c] |
| $d^3\Delta_3$–$a^3\Delta_3$ | 462.097 | 482.847 | 445.341 | 3.59 | 73.44 | −48.41 | 32, 45 |
| $d^3\Delta_2$–$a^3\Delta_2$ | 463.892 | 484.807 | 447.008 | 3.72 | 74.14 | −48.68 | 32, 45 |
| $d^3\Delta_1$–$a^3\Delta_1$ | 464.168 | 485.108 | 447.264 | 3.82 | 74.34 | −48.65 | 32, 45 |
| $c^3\Pi_2$–$a^3\Delta_3$ | 572.262 | 604.428 | 546.058 | 4.16 | 113.57 | −76.29 | 32, 45 |
| $c^3\Pi_1$–$a^3\Delta_2$ | 563.279 | 594.416 | 537.876 | 4.20 | 110.02 | −73.87 | 32, 45 |
| $c^3\Pi_0$–$a^3\Delta_1$ | 555.485 | 585.744 | 530.765 | 4.24 | 107.01 | −71.78 | 32, 45 |
| $b^3\Phi_4$–$a^3\Delta_3$ | 623.390 | 661.754 | 592.092 | 4.39 | 135.51 | −91.38 | 32, 44, 45 |
| $b^3\Phi_3$–$a^3\Delta_2$ | 635.001 | 674.853 | 602.557 | 4.75 | 141.15 | −94.46 | 32, 44, 45 |
| $b^3\Phi_2$–$a^3\Delta_1$ | 647.977 | 689.527 | 614.228 | 5.15 | 147.58 | −97.97 | 32, 44, 45 |
| $E^1\Sigma^+$–$X^1\Sigma^+$ | 368.267 | 381.885 | 357.28 | 2.83 | 48.18 | −31.61 | 33, 42, 43 |
| $D^1\Delta$–$A^1\Delta$ | 518.736 | 545.171 | 497.308 | 4.10 | 93.91 | −62.20 | 45 |
| $B^1\Pi$–$X^1\Sigma^+$ | 649.814 | 693.446 | 615.678 | 7.77 | 157.65 | −96.19 | 45 |

[a]Energy for all electronic energy levels are taken from Davis and Hammer (ref 38). [b]$\rho$ value reported by Simard et al. (ref 33) was used for the calculation of isotopic shift. [c]References for the vibrational and rotational spectroscopic constants.

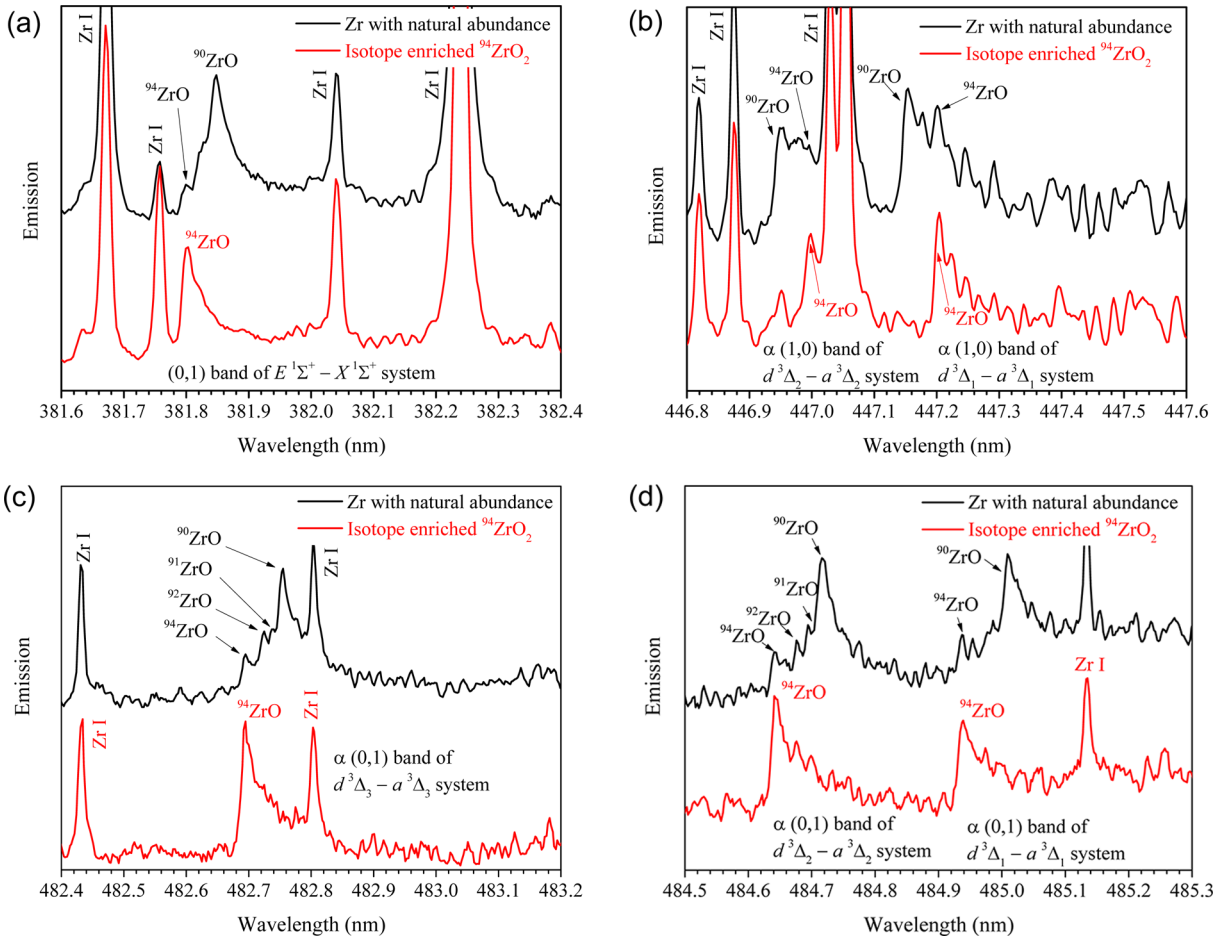


**Figure 4.** Rescaled emission spectra from laser ablation of a zirconium metal and a $^{94}ZrO_2$ pellet sample. The spectra of the two samples are offset for clarity.

to-background ratio of the molecular band and minimum spectral interference from Zr I line, an optimized gate delay of 2 $\mu$s with a gate width of 4 $\mu$s was selected for LAMIS measurements of ZrO molecular bands.

**LAMIS Analysis.** *LAMIS Spectra and Isotopic Shift Analysis.* The natural isotopic abundance of zirconium is 52.45% $^{90}$Zr, 11.22% $^{91}$Zr, 17.15% $^{92}$Zr, 17.38% $^{94}$Zr, and 2.80% $^{96}$Zr.[41] The three ZrO molecule bands presented in Figure 2 all belong to the $\alpha(0,0)$ transition (i.e., $\Delta\nu = \nu' - \nu'' = 0$), and isotopic splitting was not resolved in our measurement. Electronic transition involving a change in $\Delta\nu$ (i.e., when $\nu' \neq \nu''$) results in larger isotopic shifts (cf. eq 1). The availability of various spectroscopic (most importantly electronic and vibrational) constants[32,33,38,42−45] of ZrO allows the prediction of the band origins as well as isotopic shifts of various dipole-allowed ZrO electronic transitions. Table 1 summarizes such


DOI: 10.1021/acs.analchem.5b00056
*Anal. Chem.* 2015, 87, 4788−4796

predictions for various ZrO molecular bands with $\Delta\nu = 0, \pm 1$. Clearly, isotopic shifts in either the (0,1) or the (1,0) bands are significantly larger (by at least 1 order of magnitude) than the (0,0) counterparts. Afaf[43] reported other ZrO bands with $\Delta\nu > 1$ [e.g., the $\alpha$(2,0) and the $\alpha$(3,1) bands]. However, none of those bands with $\Delta\nu > 1$ was observed clearly in our LAMIS study.

To locate the optimum ZrO molecular band for isotopic analysis, all the predicted ZrO bands with $\Delta\nu = \pm 1$ were experimentally measured. However, only six of them exhibit clear isotopic shifts (which are shown in Figure 4), whereas other bands are either too weak or heavily blended with other spectral structures. The isotopic assignments were confirmed with an isotopically enriched Zr sample (a $ZrO_2$ pellet with 97+% $^{94}$Zr). Due to the different physical nature of the two samples (a Zr metal plate and a $ZrO_2$ powder pressed pellet), their emission intensities are not directly comparable; therefore, the intensities presented in Figure 4 are rescaled so that the candidate bandheads are similar in intensities.

Figure 4a presents the (0,1) band of the $E^1\Sigma^+ - X^1\Sigma^+$ system in the wavelength range from 381.6 to 382.4 nm. The two bandheads from $^{94}$ZrO and $^{90}$ZrO are identified with certainty, but the other two heads from $^{92}$ZrO and $^{91}$ZrO are not distinct because of their comparatively small isotope shifts. Through spectroscopic constants,[42,43] the predicted isotopic shifts for the bandheads of $^{94}$ZrO, $^{92}$ZrO, $^{91}$ZrO, with respect to that of $^{90}$ZrO, are 47, 24, 12 pm, respectively. The experimental determined isotopic shifts for $^{94}$ZrO was 45 pm and agreed well with prediction. Compared to the spectral resolution of ~15 pm of our experimental system, the $^{92}$ZrO and $^{91}$ZrO bandheads with adjacent isotopic shifts of only 12 pm could be difficult to assign with confidence.

Figure 4b depicts the $\alpha$(1,0) bands of the $d^3\Delta_2 - a^3\Delta_2$ and $d^3\Delta_1 - a^3\Delta_1$ subsystems; we also examined the wavelength region for the $\alpha$(1,0) $d^3\Delta_3 - a^3\Delta_3$ subsystem but could not confirm its presence. Similar to Figure 4a, only the bandheads from $^{90}$ZrO and $^{94}$ZrO can be unambiguously assigned. The experimentally measured wavelength differences between the $^{94}$ZrO and $^{90}$ZrO bandheads of the $d^3\Delta_2 - a^3\Delta_2$ and $d^3\Delta_1 - a^3\Delta_1$ subsystems were both 50 pm and matched well with prediction. These two subsystems suffer severe spectral interferences, and therefore, are not good candidates for LAMIS. For the $d^3\Delta_2 - a^3\Delta_2$ band, there are two strong Zr atomic lines overlap with the wing of the $^{94}$ZrO bandhead. Also, the heads of the two subsystems are very close (~0.2 nm); thus, a large fraction of the tail from the $d^3\Delta_2 - a^3\Delta_2$ band enters the bandhead of the $d^3\Delta_1 - a^3\Delta_1$ subsystem. This mutual spectral overlap from the two molecular subsystems degrades the accuracy of isotopic analysis.

The experimental $\alpha$(0,1) band spectra of the $d^3\Delta - a^3\Delta$ system are presented in Figure 4, parts c and d. The $^{90}$ZrO molecular emission with bandheads at 482.75, 484.72, 485.01 nm belong to the $\alpha$(0,1) band, and are assigned to the $d^3\Delta_3 - a^3\Delta_3$, $d^3\Delta_2 - a^3\Delta_2$, and $d^3\Delta_1 - a^3\Delta_1$ subsystems, respectively. Bandheads from $^{94}$ZrO, $^{92}$ZrO, $^{91}$ZrO, and $^{90}$ZrO can be unambiguously assigned for the $d^3\Delta_3 - a^3\Delta_3$ and the $d^3\Delta_2 - a^3\Delta_2$ subsystems. However, for the $d^3\Delta_1 - a^3\Delta_1$ subsystem, only the $^{94}$ZrO and $^{90}$ZrO bandheads are identified with certainty, whereas the heads for $^{91}$ZrO and $^{92}$ZrO are probably distorted due to spectral interferences from the tails of the $d^3\Delta_2 - a^3\Delta_2$ and the $d^3\Delta_3 - a^3\Delta_3$ subsystems. In all cases, the bandhead from $^{96}$ZrO could not be identified with certainty due to the highly structural baseline resulting from the rotational structures of other nearby ZrO bands[43] and the comparatively low abundance of $^{96}$Zr (2.8%).

Figure 5 shows the isotopic shifts, with respect to $^{90}$ZrO, of the $^{91}$ZrO, $^{92}$ZrO, and $^{94}$ZrO bandheads of the three $\alpha$(0,1)

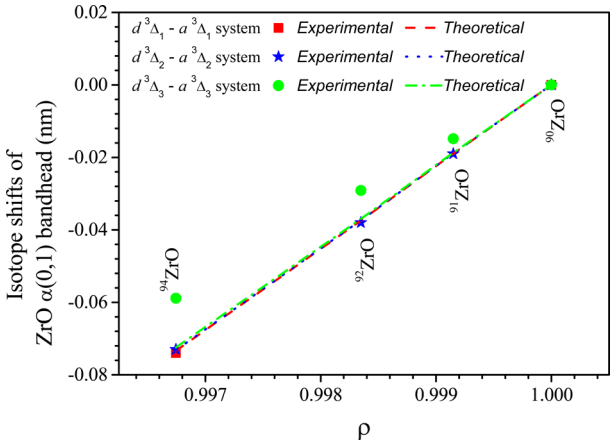


**Figure 5.** Predicted and experimentally measured isotopic shifts for the ZrO $\alpha$(0,1) bandheads, referenced to $^{90}$ZrO. The experimental observed shifts in the $d^3\Delta_2 - a^3\Delta_2$ and $d^3\Delta_1 - a^3\Delta_1$ subsystems agree well with theoretical prediction. In contrast, notable deviation from the predicted values were observed for the $d^3\Delta_3 - a^3\Delta_3$ subsystem.

subsystems. Because the vibrational and rotational constants of these three subsystems are very similar,[31,32] their isotopic shifts should be practically identical (cf. eq 1). The isotopic shifts of the $d^3\Delta_2 - a^3\Delta_2$ and $d^3\Delta_1 - a^3\Delta_1$ subsystems agree well with the theoretical prediction (with $\rho$ values from Simard et al.[33]), whereas the $d^3\Delta_3 - a^3\Delta_3$ subsystem exhibits a systematic deviation. The theoretical isotopic shift from $^{90}$ZrO to $^{94}$ZrO is 72 pm, whereas the experimental measured one is only 59 pm for the $d^3\Delta_3 - a^3\Delta_3$ subsystem. Since the predicted isotopic shift strongly depends on the molecular spectroscopic constants (eq 1), we checked the employed molecular spectroscopic constants and found that they fit very well for the $\alpha$(0,0) band, thus ruling out the possibility that the disagreement in isotopic shifts is due to an uncertainty in the vibrational or rotational constant. The wavelength was calibrated with a Fe–Ne hollow cathode lamp, and the curvature on the focal plane of our Czerny–Turner spectrometer[27] was also corrected. We concluded that this 13 pm difference in isotopic shift is significant.

Although not common, deviations of the experimental isotope shifts from theoretical values predicted from the spectroscopic constants and reduced mass of the molecule (eq 1) have been reported in the literature.[46,47] One reason for such deviation is perturbation of energy levels.[46] Afaf[48] reported some abnormality of the energy levels in the $d^3\Delta_3$ state (the old convention $C^3\Delta_3$ was used in his work) of ZrO. Specifically, he stated that there is energy-level crossing from another $^3\Delta_3$ repulsive state to this $d^3\Delta_3$ level, leading to a potential maximum in the $d^3\Delta_3$ state. He further reported that similar potential maxima have not been observed in the other two sublevels—the $d^3\Delta_2$ and $d^3\Delta_1$.[48] We, therefore, attribute the deviations of the isotope shifts of the $d^3\Delta_3 - a^3\Delta_3$ (0,1) band to perturbation in the upper energy level.

As all the three $\alpha$(0,1) bands are degraded to red, the $d^3\Delta_3 - a^3\Delta_3$ subsystem, whose bandhead is located at the lowest wavelength among the three, is the only one that does not


DOI: 10.1021/acs.analchem.5b00056
Anal. Chem. 2015, 87, 4788–4796

suffer from spectral interferences from the other two $\alpha(0,1)$ bands. Although the isotope shifts in the $\alpha(0,1)$ $d^3\Delta_2$–$a^3\Delta_2$ subsystem are better resolved, a close-by Zr I line (only ~8 pm away) could potentially interfere with the band head of $^{94}$ZrO. In the series of emission spectra taken at different delay times shown in Figure 6, it is clear that emission from this Zr I line is

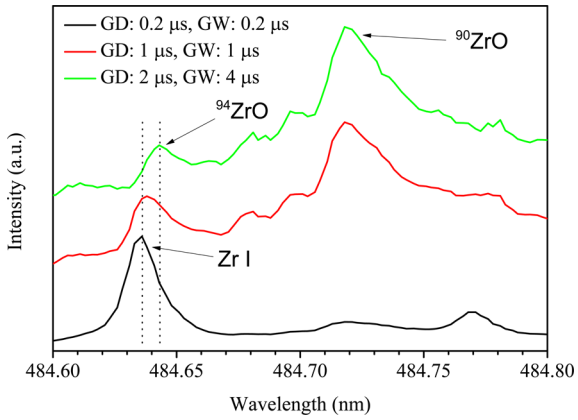


**Figure 6.** Emission spectra of the $\alpha(0,1)$ $d^3\Delta_2$–$a^3\Delta_2$ subsystem acquired with different delay times. Intensities were rescaled for clarity.

strong at early delay time. Comparing spectra obtained at 1 and 2 $\mu$s delays, there is a distinct shift in the $^{94}$ZrO bandhead due to spectral interference. Therefore, despite a perturbation in the $d^3\Delta_3$ energy level, the $d^3\Delta_3$–$a^3\Delta_3$ subsystem was chosen for isotopic analysis. To account for the effect on the isotopic shifts from the aforementioned energy-level perturbation, we tuned the $\rho$ values for each Zr isotope based on our experimental spectra to generate the synthetic spectra for the fitting.

*Semiquantitative Isotopic Analysis for Zr.* There are two common approaches for the calibration of LAMIS signals—through multivariate calibration with a set of isotopic-enriched calibration standards or through fitting of experimental spectrum by simulated molecular spectra model.[8,35] We selected the fitting approach because isotopically enriched standards, in the same form as our sample (i.e., metal), are not commercially available. In the present study, we neglected the contributions from the tails of other nearby bands [e.g., the $\alpha(0,0)$ band shown in Figure 2 and the singlet C(0,1) band at ~473.69 nm[43]]. In addition, we also neglected $^{96}$ZrO and the possible hyperfine structures in $^{91}$ZrO.[49,50] Therefore, this isotopic analysis is semiquantitative in nature. An optimized gate delay of 2 $\mu$s with a gate width of 4 $\mu$s was used, based on a compromise between maximum signal-to-background ratio of the molecular band and minimum spectral interference from the Zr I line. The total data-acquisition time for each spectrum was 5 s (i.e., 5000 laser pulses).

Figure 7 represents the experimental spectrum and its fitting with simulated spectra model for the $\alpha(0,1)$ bands of the $d^3\Delta_3$–$a^3\Delta_3$ subsystem from 482.67 to 482.82 nm. In this example, the determined ratio of $^{90}$Zr/$^{91}$Zr/$^{92}$Zr/$^{94}$Zr was 2.86:0.47:1.20:1. The Zr isotope ratios determined from a Zr metal sample with natural isotopic abundance, together with the theoretical abundance ratios, are summarized in Table 2. The determined $^{90}$Zr/$^{94}$Zr ratios agree well with the natural abundance value. In contrast, the $^{91}$Zr/$^{94}$Zr ratios deviate significantly from the natural abundance value. The low abundance of $^{91}$Zr could be one reason, but the hyperfine structure in the molecular emission of $^{91}$ZrO is another

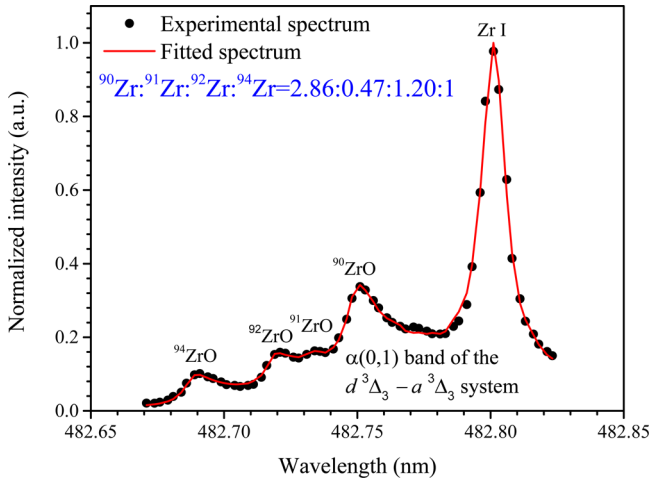


**Figure 7.** Experimentally acquired spectrum and its fitting with simulated spectra model. Gate delay and width of the ICCD were 2 and 4 $\mu$s, respectively. Measurement time was 5 s (corresponded to 5000 laser shots).

**Table 2. Ratios of Zirconium Isotopes Determined from the $d^3\Delta_3$–$a^3\Delta_3$ Subsystem of the ZrO $\alpha(0,1)$ Molecular Band by fs-LAMIS[a]**

| Zr isotopes | ratios of natural abundance | fs-LAMIS |
|---|---|---|
| $^{94}$Zr | 1 | 1 |
| $^{92}$Zr | 0.987 | 1.16 ± 0.06 |
| $^{91}$Zr | 0.646 | 0.47 ± 0.03 |
| $^{90}$Zr | 2.960 | 2.93 ± 0.08 |

[a]An acquisition time of 5 s was employed for each measurement. The uncertainties represent the standard deviations of 10 measurements.

potential cause. The effect of hyperfine structure is a splitting of the energy levels, and hence a splitting of the spectral lines; as a result, the individual components inside a molecular band become more spread out and the overall molecular emission appears weaker.[49] Although there is no information in the literature specifically for the $\alpha(0,1)$ band, hyperfine structures in molecular bands of ZrO have been reported.[49,51] If hyperfine structures exist in the $\alpha(0,1)$ system of $^{91}$ZrO, a lower determined $^{91}$Zr/$^{94}$Zr ratio could result. The hyperfine structure depends on the exact coupling scheme between the different angular momentums and the associated hyperfine constants,[52] which are both unknown for the $\alpha(0,1)$ system of $^{91}$ZrO. Knowledge of these constants would help to improve the accuracy of isotopic determination.

The accuracy of the Zr isotopic analysis by LAMIS is not as good as those previously reported[8,11] for other elements. The main reason is that a different calibration methodology was used in this work. In our previous LAMIS works[8,11] (e.g., $^{11}$BO/$^{10}$BO and HO/DO), isotopic calibrations were performed with partial least-squares (PLS) regression, which requires the availability of a set of isotope-enriched standards. The effects of any perturbations in energy levels or hyperfine splitting on the molecular spectra will be taken care of during the calibration process. Therefore, the analytical performance is good as long as the ablation and plasma behavior does not vary considerably between calibration and sample analysis. Here, we emphasized a standardless calibration approach through theoretical spectral fitting. The analytical accuracy is degraded by this approach because not all the effects (e.g., perturbation,


DOI: 10.1021/acs.analchem.5b00056
Anal. Chem. 2015, 87, 4788–4796

hyperfine splitting, and spectral overlap with other bands) are taken into account due to a lack of such information. On the other hand, when spectroscopic constants for these effects become available, it is possible to implement them into the fitting algorithm, which can subsequently improve the analytical accuracy of this standardless approach.

## CONCLUSION

The emission characteristics and analytical performance of isotopic analysis by LAMIS with the use of high repetition rate, low pulse-energy femtosecond pulses was studied. The temporally resolved emission intensities of atomic/ionic lines and molecular bands were characterized, and the results showed that the molecular band to atomic line intensity ratio increases as the plasma decays. All the measurable molecular bands and their isotope shifts were examined experimentally and theoretically. The $\alpha(0,1)$ band of $d^3\Delta_3-a^3\Delta_3$ subsystem was selected for isotope ratio analysis with a standardless calibration approach—by fitting the experimental acquired molecular spectra with a set of theoretical synthetic spectra.

This work also underlines the critical need of comprehensive molecular constants for LAMIS, including information on energy-level perturbations, vibrational and rotational constants of nearby bands, and hyperfine constants. We found that the isotope shifts in the ZrO $\alpha(0,1)$ bands of the $d^3\Delta_3-a^3\Delta_3$ subsystem appreciably differ from the predicted values, which could be attributed to a perturbation in the energy level of the $d^3\Delta_3$ state. Also, the availability of accurate spectroscopic constants is needed to generate the synthetic spectrum for spectral fitting. For example, rotational constants for both the upper and lower levels of the singlet C(0,1) band (with bandhead at ~473.69 nm[43]) are not available in the literature. The tail of this C(0,1) band likely enters the $\alpha(0,1)$ system and, therefore, would impair the accuracy of isotopic analysis if neglected. The hyperfine structure could distort the spectral shape and again could degrade the accuracy. Inclusion of all these effects into the fitting algorithm is possible only if their spectroscopic constants are available. Nevertheless, without taking into account of these potential effects, LAMIS can readily provide semiquantitative isotopic analysis without sample preparation and without an isotopically labeled calibration standard, as demonstrated in this work.

## AUTHOR INFORMATION

### Corresponding Author

*E-mail: rerusso@lbl.gov.

### Notes

The authors declare no competing financial interest.

## ACKNOWLEDGMENTS

The research was supported by the U.S. Department of Energy, Office of Nuclear Nonproliferation, under contract no. DEAC02-05CH112 at the Lawrence Berkeley National Laboratory. Huaming Hou acknowledges support from the China Scholarship Council (CSC).

## REFERENCES

(1) Hahn, D. W.; Omenetto, N. *Appl. Spectrosc.* **2010**, *64*, 335A–366A.
(2) Hou, H.; Tian, Y.; Li, Y.; Zheng, R. *J. Anal. At. Spectrom.* **2014**, *29*, 169–175.
(3) Baudelet, M.; Smith, B. W. *J. Anal. At. Spectrom.* **2013**, *28*, 624–629.
(4) Hahn, D. W.; Omenetto, N. *Appl. Spectrosc.* **2012**, *66*, 347–419.
(5) Cremers, D.; Beddingfield, A.; Smithwick, R.; Chinni, R. C.; Jones, C. R.; Beardsley, B.; Karch, L. *Appl. Spectrosc.* **2012**, *66*, 250–261.
(6) Russo, R. E.; Bol'shakov, A.; Mao, X.; McKay, C. P.; Perry, D. L.; Sorkhabi, O. *Spectrochim. Acta, Part B* **2011**, *66*, 99–104.
(7) Mao, X.; Bol'Shakov, A. A.; Choi, I.; McKay, C. P.; Perry, D. L.; Sorkhabi, O.; Russo, R. E. *Spectrochim. Acta, Part B* **2011**, *66*, 767–775.
(8) Sarkar, A.; Mao, X.; Russo, R. E. *Spectrochim. Acta, Part B* **2014**, *92*, 42–50.
(9) Ko, P.; Jovanovic, I. *Spectrochim. Acta, Part B* **2013**, *90*, 68–71.
(10) Mao, X.; Bol'shakov, A.; Perry, D. L.; Sorkhabi, O.; Russo, R. E. *Spectrochim. Acta, Part B* **2011**, *66*, 604–609.
(11) Sarkar, A.; Mao, X.; Chan, G. C.-Y.; Russo, R. E. *Spectrochim. Acta, Part B* **2013**, *88*, 46–53.
(12) Boumans, P. W. J. M. *Fresenius' Z. Anal. Chem.* **1986**, *324*, 397–425.
(13) Boumans, P. W. J. M. *Anal. Chem.* **1994**, *66*, 459A–467A.
(14) Krishna, G. R.; Ravindra, H. R.; Gopalan, B.; Syamsunder, S. *Anal. Chim. Acta* **1995**, *309*, 333–338.
(15) Simonits, A.; Corte, F.; Hoste, J. *J. Radioanal. Chem.* **1976**, *31*, 467–486.
(16) Robertson, J. A. L. *J. Nucl. Mater.* **1981**, *100*, 108–118.
(17) Northwood, D. O. *Mater. Des.* **1985**, *6*, 58–70.
(18) Loveland, W. D.; Morrissey, D. J.; Seaborg, G. T. *Modern Nuclear Chemistry*; John Wiley & Sons: Hoboken, NJ, 2006; pp 299–330.
(19) Lieser, K. H. *Nuclear and Radiochemistry: Fundamentals and Applications*; Wiley-VCH: Weinheim, Germany, 2001; pp 127–170.
(20) Smułek, W.; Al-Dabbagh, R. K.; Goroncek, K.; Borkowski, M. *J. Radioanal. Nucl. Chem.* **1988**, *121*, 385–393.
(21) Becker, J. S.; Dietze, H.-J. *Spectrochim. Acta, Part B* **1998**, *53*, 1475–1506.
(22) Ireland, T. R. *Rev. Sci. Instrum.* **2013**, *84*, 011101.
(23) Langlois, E.; Gagné, J.-M. *J. Opt. Soc. Am. B* **1994**, *11*, 552–557.
(24) Sunku, S.; Gundawar, M. K.; Myakalwar, A. K.; Kiran, P. P.; Tewari, S. P.; Rao, S. V. *Spectrochim. Acta, Part B* **2013**, *79–80*, 31–38.
(25) Dikmelik, Y.; McEnnis, C.; Spicer, J. B. *Opt. Express* **2008**, *16*, 5332–5337.
(26) Baudelet, M.; Guyon, L.; Yu, J.; Wolf, J.-P.; Amodeo, T.; Fréjafon, E.; Laloi, P. *J. Appl. Phys.* **2006**, *99*, 084701.
(27) Peláez, R. J.; Mar, S.; Aparicio, J. A.; Belmonte, M. T. *Appl. Spectrosc.* **2012**, *66*, 970–978.
(28) Crosswhite, H. *J. Res. Natl. Bur. Stand., Sect. A* **1975**, *79A*, 17–69.
(29) Mulliken, R. *Phys. Rev.* **1925**, *25*, 119–138.
(30) Birge, R. T. *Trans. Faraday Soc.* **1929**, *25*, 0718–0724.
(31) Afaf, M. *Proc. Phys. Soc., London, Sect. A* **1950**, *63*, 1156–1170.
(32) Kaledin, L. A.; Mccord, J. E.; Heaven, M. C. *J. Mol. Spectrosc.* **1995**, *174*, 93–99.
(33) Simard, B.; Mitchell, S. A.; Humphries, M. R.; Hackett, P. A. *J. Mol. Spectrosc.* **1988**, *129*, 186–201.
(34) Ochkin, V. N. *Spectroscopy of Low Temperature Plasma*, 1st ed.; Wiley-VCH: Weinheim, Germany, 2009; pp 569–582.
(35) Dong, M.; Mao, X.; Gonzalez, J. J.; Lu, J.; Russo, R. E. *Anal. Chem.* **2013**, *85*, 2899–2906.
(36) Dong, M.; Chan, G. C.-Y.; Mao, X.; Gonzalez, J. J.; Lu, J.; Russo, R. E. *Spectrochim. Acta, Part B* **2014**, *100*, 62–69.
(37) Cravetchi, I. V.; Taschuk, M. T.; Tsui, Y. Y.; Fedosejevs, R. *Anal. Bioanal. Chem.* **2006**, *385*, 287–294.
(38) Davis, S. P.; Hammer, P. D. *Astrophys. J.* **1988**, *332*, 1090–1091.
(39) Afaf, M. *Astrophys. J.* **1995**, *447*, 980–983.
(40) Bai, X.; Motto-Ros, V.; Lei, W.; Zheng, L.; Yu, J. *Spectrochim. Acta, Part B* **2014**, *99*, 193–200.
(41) Berglund, M.; Wieser, M. E. *Pure Appl. Chem.* **2011**, *83*, 397–410.
(42) Afaf, M. *Nature* **1949**, *164*, 752–753.
(43) Afaf, M. *Astrophys. J.* **1987**, *314*, 415–418.



DOI: 10.1021/acs.analchem.5b00056
*Anal. Chem.* 2015, 87, 4788–4796

(44) Tatum, J. B.; Balfour, W. J. *J. Mol. Spectrosc.* **1973**, *48*, 292−312.
(45) NIST Standard Reference Database Number 69. http://webbook.nist.gov/chemistry/ (accessed June 1, 2014).
(46) Mi Hamrick, Y.; Taylor, S.; Morse, M. D. *J. Mol. Spectrosc.* **1991**, *146*, 274−313.
(47) Garcia, M. A.; Vietz, C.; Ruipérez, F.; Morse, M. D.; Infante, I. *J. Chem. Phys.* **2013**, *138*, 154306.
(48) Afaf, M. *Astrophys. J.* **1988**, *324*, 1219−1220.
(49) Littleton, J. E.; Davis, S. P. *Astrophys. J.* **1985**, *296*, 152−159.
(50) Simard, B.; Mitchell, S. A.; Hendel, L. M.; Hackett, P. A. *Faraday Discuss. Chem. Soc.* **1988**, *86*, 163−180.
(51) Simard, B.; Mitchell, S. *Faraday Discuss.* **1988**, *86*, 163−180.
(52) Rao, K. N.; Mathews, C. W. *Mol. Spectrosc.: Mod. Res.* **1972**, 231−257.



DOI: 10.1021/acs.analchem.5b00056
*Anal. Chem.* 2015, 87, 4788−4796